Redox Biology 69 (2024) 102998

Contents lists available at ScienceDirect

Redox Biology

journal homepage: www.elsevier.com/locate/redox

Fibroblast growth factor receptor-4 mediates activation of Nuclear Factor Erythroid 2-Related Factor-2 in gastric tumorigenesis

Mohammed Soutto [a,b], Xing Zhang [c,d], Nadeem Bhat [b], Zheng Chen [b], Shoumin Zhu [b], Selma Maacha [b], Melanie Genoula [b], Omar El-Gazzaz [b], Dunfa Peng [b], Heng Lu [b], Oliver G. McDonald [e], Xi Steven Chen [f], Longlong Cao [g], Zekuan Xu [c,h], Wael El-Rifai [a,b,*]

[a] *Department of Veterans Affairs, Miami Healthcare System, Miami, FL, USA*
[b] *Department of Surgery, University of Miami Miller School of Medicine, Miami, FL, 33136, USA*
[c] *Department of General Surgery, The First Affiliated Hospital of Nanjing Medical University, Nanjing, Jiangsu, 210029, China*
[d] *Department of Thoracic Surgery, Jiangsu Cancer Hospital, Jiangsu Institute of Cancer Research, The Affiliated Cancer Hospital of Nanjing Medical University, Nanjing, Jiangsu, 210009, China*
[e] *Department of Pathology, University of Miami Miller School of Medicine, Miami, FL, 33136, USA*
[f] *Division of Biostatistics, Department of Public Health Science, Sylvester Comprehensive Cancer Center, University of Miami Miller School of Medicine, Miami, FL, 33136, USA*
[g] *Department of Gastric Surgery, Fujian Medical University Union Hospital, Fuzhou, China*
[h] *Jiangsu Key Lab of Cancer Biomarkers, Prevention and Treatment, Jiangsu Collaborative Innovation Center for Cancer Personalized Medicine, School of Public Health, Nanjing Medical University, Nanjing, Jiangsu, 211166, China*

A B S T R A C T

Helicobacter pylori (H. pylori) is the leading risk factor for gastric carcinogenesis. Fibroblast growth factor receptor 4 (FGFR4) is a member of transmembrane tyrosine kinase receptors that are activated in cancer. We investigated the role of FGFR4 in regulating the cellular response to *H. pylori* infection in gastric cancer. High levels of oxidative stress signature and FGFR4 expression were detected in gastric cancer samples. Gene set enrichment analysis (GSEA) demonstrated enrichment of NRF2 signature in samples with high FGFR4 levels. *H. pylori* infection induced reactive oxygen species (ROS) with a cellular response manifested by an increase in FGFR4 with accumulation and nuclear localization NRF2. Knocking down FGFR4 significantly reduced NRF2 protein and transcription activity levels, leading to higher levels of ROS and DNA damage following *H. pylori* infection. We confirmed the induction of FGFR4 and NRF2 levels using mouse models following infection with a mouse-adapted *H. pylori strain*. Pharmacologic inhibition of FGFR4 using H3B-6527, or its knockdown, remarkably reduced the level of NRF2 with a reduction in the size and number of gastric cancer spheroids. Mechanistically, we detected binding between FGFR4 and P62 proteins, competing with NRF2-KEAP1 interaction, allowing NRF2 to escape KEAP1-dependent degradation with subsequent accumulation and translocation to the nucleus. These findings demonstrate a novel functional role of FGFR4 in cellular homeostasis via regulating the NRF2 levels in response to *H. pylori* infection in gastric carcinogenesis, calling for testing the therapeutic efficacy of FGFR4 inhibitors in gastric cancer models.

1. Introduction

Gastric cancer is the fifth most common cancer worldwide, with an estimated 26,380 new cases and 11,090 deaths in the United States in 2022 [1,2]. In addition to lifestyle and genetic risk factors, *Helicobacter pylori (H. pylori)* infection remains the strongest known risk factor for gastric carcinogenesis [3]. Infection with *H. pylori* induces high levels of reactive oxygen species and oxidative stress in gastric epithelial cells [4,5], necessitating the activation of antioxidant mechanisms to maintain ROS below the lethal levels and counteract the cellular genotoxic effects of oxidative stress.

Nuclear Factor Erythroid 2-Related Factor 2 (NRF2) is a transcription factor that plays a critical role in the antioxidant response. NRF2 transcription targets include a cytoprotective gene battery that protects against oxidative and cellular stress [6,7]. Under normal physiological conditions, NRF2 is rapidly induced in response to stress with a short half-life, where KEAP1 (Kelch-like ECH-associated protein 1) protein mediates its ubiquitination and proteasomal degradation via Cullin 3-based E3 ubiquitin ligase [8]. P62, also known as SQSTM1, can compete with NRF2 by interacting with KEAP1 leading to decreased NRF2 ubiquitination with subsequent accumulation, nuclear translocation, and transcription activation [9].

* Corresponding author. Department of Veterans Affairs, Miami Healthcare System, Miami, FL, USA.
E-mail address: welrifai@med.miami.edu (W. El-Rifai).

https://doi.org/10.1016/j.redox.2023.102998
Received 15 November 2023; Accepted 13 December 2023
Available online 19 December 2023

Fibroblast growth factor receptors 4 (FGFR4) belongs to a tyrosine kinase family that includes three other highly conserved receptors (FGFR1, FGFR2 and FGFR3) [10,11]. FGFRs regulate essential cancer processes, including cellular development, motility, survival, and angiogenesis [12,13]. Aberrant activation of FGFRs has been implicated in the development and progression of multiple cancers, including gastric cancer [10]. The activation of FGFR4 in several human cancers is closely associated with its specific ligand, FGF19 [14,15]. In mice, *Fgf15*, the ortholog of human *FGF19*, has been shown to be an important contributor to hepatocarcinogenesis [16], where its knockdown resulted in reduced tumor progression [16]. The FGF ligand binds to the FGFR4 receptor to form a dimer leading to FGFR4 autophosphorylation in the intracellular kinase domain. FGFR4 mediates activation of several oncogenic signaling pathways, including Wnt/β-Catenin [17], PI3K-AKT [18] and RAS-RAF-ERK [19]. A recent study has shown that *H. pylori* induces FGF19 and FGFR4 with subsequent activation of FGFR4 signaling [15]. However, the spectrum of FGFR4 functions in response to *H. pylori* infection remains largely unexplored.

In this study, we investigated the function of FGFR4 in gastric cancer and determined its role in the activation of NRF2 in response to *H. pylori*. The results demonstrated that FGFR4 plays an important role in the stabilization, nuclear accumulation, and activation of NRF2. This activation was mediated by blocking ubiquitination and proteasomal degradation of NRF2 by KEAP1 via a physical interaction between FGFR4, KEAP1, and P62.

2. Materials and methods

2.1. Animals study

All animal procedures were approved by the Institutional Animal Care and Use Committees at the University of Miami (IACUC 20-110). Wild-type C57/B6 (WT) and TFF1-Knockout mice (TFF1-KO) [20,21] were used to investigate the association between FGFR4, NRF2 and *H. pylori* in gastric tumorigenesis. WT and TFF1-KO mice were assigned into two groups. Mice in the experimental group were challenged with mouse adapted *H. pylori* PMSS1 strain (10^9 CFU/mouse) via orogastric gavage. Mice in the control group received Brucella broth alone. Mice were euthanized four weeks after infection. Stomachs were cut along the lesser curvature, washed with PBS, and opened to lie flat. The stomachs were examined visually for abnormalities, the size, and number of individual gastric tumors and photographed. Each stomach was cut into symmetrical halves. One half was submerged in 10 % buffered formalin solution, embedded in paraffin, and processed for standard H&E staining for histopathology evaluation. The antro-pyloric region of the second half of the stomach was snap-frozen and stored at −80 °C.

2.2. Cell culture and reagents

Human gastric cell lines included AGS, MKN28, MKN45, and GES1 cells. The MKN28 and MKN45 were purchased from Riken Cell Bank (Tsukuba, Japan). AGS and cells were purchased from American Tissue Culture Collection (ATCC, Manassas, VA), whereas GES1 Human gastric epithelial cell line was a gift from Dr. Kidane-Mulat (University of Texas-Austin). Cells were cultured Following the recommended culture medium, RPMI 1640 medium (Thermofisher Scientific, USA) or F12 Ham medium (Thermofisher Scientific, USA), with 10 % fetal bovine serum (Thermofisher Scientific, USA) and 1 % penicillin/streptomycin (Thermofisher Scientific, USA). In addition, the recombinant human fibroblast growth factor 19 (FGF19) was purchased from Thermofisher Scientific (Thermofisher Scientific, USA).

2.3. *In vitro studies of* *H. pylori* infection

In the *in vitro* study, we used two *H. pylori* strains, J166 and 7.13. J166 is a human-derived *H. pylori*, and 7.13 *H. pylori* is a carcinogenic gerbil-adapted strain derived from the human B128 *strain*. All strains are *CagA* + types and were obtained from Dr. Richard Peek, Jr. (Vanderbilt University Medical Center). The cultures of *H. pylori* were made on Brucella agar (BBL/Becton Dickinson, Sparks, MD) supplemented with 5 % heat-inactivated BSA (Thermofisher Scientific, USA) and a combination of antibiotics (vancomycin, 100 μg/ml; bacitracin, 200 μg/ml; amphotericin B, 20 μg/ml; nalidixic acid, 10.7 μg/ml; polymyxin B, 3.3 μg/ml) (Sigma-Aldrich, St. Louis, MO). *H. pylori* cultures from inoculation were grown in Brucella broth supplemented with 10 % BSA and vancomycin antibiotic. After 24 h, bacteria were pelleted and resuspended in PBS. Epithelial cells were infected by *H. pylori* at a multiplicity of infection (MOI) of 50:1 [22,23].

2.4. FGFR4 knockdown and overexpression

For the knockdown, AGS, MKN28 and GES1 cells were transfected for 48 h with a universal negative control siRNA (Sigma–Aldrich) or FGFR4 siRNA (Thermofisher Scientific) using LipoJet (SignaGen Laboratories). After 48h, cells were infected with *H. pylori* or stimulated with recombinant FGF19 recombinant protein. For FGFR4 overexpression, the pHAGE-FGFR4 plasmid was purchased from Addgene (Watertown, MA). The pcDNA3 empty vector was used as a control.AGS and MKN28 cells were transiently transfected with (1 μg) of FGFR4 plasmid or control vector using PolyJet transfection reagent (SignaGen Laboratories, Frederick, MD). Fourty-8 h after transfection, cells were processed for experiments. For silencing FGFR4 in human normal gastric organoids [15], organoids were dissociated from Matrigel into single cells and transduced with FGFR4 short heparin lentiviral particles in the presence of 8 μg/ml polybrene (Sigma-Aldrich). After 24 h, cells were centrifuged, and the pellet was resuspended in Matrigel and cultured for recovery in IntestiCult Organoid Growth Medium. After one week, the formed organoids were treated with FGF19 (200 ng/ml) for 24h. Matrigel was dissociated, and organoids were collected and fixed in 10 % formalin. The pellet was resuspended in HistoGel and embedded in paraffin. The silencing was evaluated by Immunofluorescence.

2.5. Western blotting

Cells were collected and lysed in RIPA buffer (10 mM Tris–HCl (pH 7.2), 150 mM NaCl, 5 mM EDTA, 0.1 % sodium dodecyl sulfate (SDS), 1.0 % Triton X-100, 1 % deoxycholate) with a cocktail of protease and phosphatase inhibitors. Protein concentration was measured using Bio-Rad Protein Assay (Bio-Rad Laboratories, Hercules, CA).Ten to 15 μg of proteins were run on SDS/polyacrylamide gel electrophoresis (PAGE) and transferred onto nitrocellulose membranes (Millipore, Billerica, Massachusetts, USA). Membranes were blocked with 5 % bovine serum albumin (BSA, Sigma-Aldrich). The antibodies used for western blot analysis were: FGFR4 and HO1 (Proteintech, Chicago, IL, USA), NRF2 (Abcam, Cambridge, MA), P62, p-P62 (S349) (Cell Signaling Technology, Danvers, Massachusetts, USA). P-FGFR4 (Y642) (Thermofisher Scientific, USA). CagA (GeneTex, Inc. San Antonio, Texas) and Actin (Sigma, St Louis, MO).

2.6. Intracellular ROS detection by fluorescent microscope

MKN28 and AGS cells were cultured in 6 wells and transfected with control siRNA or FGFR4 siRNA. After 48h, cells were split and seeded at $2x10^5$ cells per well in a 24-wells plate. Next day, cells were infected with *H. pylori* J166 or 7.13 strains for 6 h and prepared for ROS assay. Cells were incubated with 0.5 μM of 5-(and-6)-chloromethyl-2′, 7′-dichlorodihydrofluorescein diacetate and acetylester (CM-H2DCFDA, Invitrogen) in DMEM phenol red free medium in dark at room temperature for 20 min, then washed with PBS. To allow de-esterification of the dye, cells were incubated at 37 °C in phenol red free DMEM (Gibco, Carlsbad, California, USA) containing 5 % serum for 15 min. Cells were fixed with 4 % paraformaldehyde for 20 min and slides were mounted ad

processed for fluorescence detection using BZX-700 microscope fluorescent microscope.

2.7. Immunofluorescence

For paraffin embedded tissue sections, the slides were deparaffinized, followed by antigen retrieval in a pressure cooker for 30 min in 1xTE buffer (pH 9). Blocking was performed for 1 h at room temperature in 5 % BSA (bovine serum albumin) in 1X PBS. Next, the tissue sections were incubated with two primary antibodies, rabbit NRF2 from Novus Biologicals and mouse FGFR4 from Santa Cruz Biotechnology, diluted in blocking buffer (1:200) overnight at 4 °C. The next day, sections were washed and incubated with secondary antibodies, goat anti-mouse IgG conjugated to Alexa Fluor 488 and goat anti-rabbit IgG conjugated to Alexa Fluor 568 (Thermofisher), diluted in blocking buffer (1:500) for 1 h at room temperature. For nuclear staining, sections were washed three times and incubated with Hoechst (10 μg/ml) for 10 min. The tissue sections were mounted, and images were captured using the Keyence BZX-700 microscope.

For MKN28 and AGS gastric cancer cell lines, FGFR4 or control siRNAs transfected cells were plated in the 8-well chambers, and infected with *H. pylori* 7.13 strain for 3h. Cells were fixed with a fresh 4 % paraformaldehyde solution for 45 min at room temperature, then washed with cold PBS. Next, we added 200ul of permeabilization solution for 30 min, then washed twice with PBS. Cells were blocked with 10 % non-immune goat serum blocking solution (Life Technologies) for 20 min.

For detection of oxidative DNA damage, mouse 8-Oxoguanine Glycosylase antibody (Thermofisher, Scientific, USA) (1:200) was added for 2 h in the dark. The 8-well chamber slides were washed with PBS three times after incubating with the first antibody. Next, 100ul of goat anti-mouse IgG conjugated to Alexa Fluor 568 (Invitrogen) (1:500) was added to each well and incubated for 1h at room temperature. Cells were washed three times with PBS and incubated with Hoechst (10 μg/ml) for 10 min. The slides were mounted, and images were captured using the Keyence BZX-700 microscope.

For NRF2 and FGFR4 detection, 100ul of (1:200) rabbit NRF2 antibody (Novus Biologicals), 1:200 mouse FGFR4 antibody (Santa Cruz Biotechnology), were added for overnight in the dark. The 8-well chamber slides were washed with PBS three times then incubated with secondary antibodies, goat anti-mouse IgG conjugated to Alexa Fluor 488 and goat anti-rabbit IgG conjugated to Alexa Fluor 568 (Invitrogen) for 1h. For nuclear staining, cells were washed three times with PBS and incubated with Hoechst (10 μg/ml) for 10 min. The slides were mounted, and images were captured using the Keyence BZX-700 microscope.

2.8. RNA extraction and RT-qPCR

Total RNA was isolated from tissues and cell lines using the RNeasy Mini kit (Qiagen), and single-stranded cDNA was subsequently synthesized using the Advantage RT-for-PCR Kit (Clontech Laboratories Inc). Mouse and human primers for specific genes were designed using the online software for primer 3 (http://frodo.wi.mit.edu/cgi-bin/primer3/primer3_www.cgi). The mouse primers for: *Fgfr4, Nrf2, Fgf15*, *Ho1 and Hprt*; The human: *FGFR4, NRF2, HO1 and HPRT* (Supplemental Table 1). All primers were purchased from (IDT) Integrated DNA Technologies (Supplemental Table 1). The RT-qPCR was performed using the CFX96 Real-Time PCR Detection System (Bio-Rad, Hercules, CA, USA), with the threshold cycle number determined using the iCycler Software version 3.0. Reactions were performed in triplicate, and the threshold cycle numbers were averaged. The results of the genes were normalized to housekeeping genes, HPRT for humans and mice. The expression ratios were calculated according to the formula $2^{(Rt-Et)}/2^{(Rn-En)}$ and the results were analyzed as described earlier [24].

2.9. Luciferase reporter assay

Briefly, MKN28 and AGS cells were cultured in 6 wells and transfected with control siRNA or FGFR4 siRNA with Lipo-Jet. After 6h, media was changed and cells were co-transfected with PGL4.37 [luc2P/ARE/Hygro] reporter (Promega, Madison, WI), as a measure of NRF2 transcription activity, along with renilla as the internal control using poly-Jet DNA transfecting agent. After 48h, cells were split and seeded at $2x10^5$ cells per well in a 24-wells plate and infected with *H. pylori* for 3h. The cells were harvested and lysed with 1X luciferase passive lysis buffer. Luciferase activity was measured after adding the luciferase reagent and renilla after adding the stop solution using a dual-luciferase reporter assay system (Promega) in a FLUOstar OPTIMA microplate reader (BMG LABTECH, Cary, NC). Luciferase activity was calculated by normalizing the luciferase with the corresponding renilla value and represented as relative luciferase activity (RLU).

2.10. Proximity ligation assay

MKN28 gastric cancer cells were transfected with FGFR4 siRNA or control siRNAs. Cells were plated in 8-well chambers and infected with *H. pylori* 7.13 strain for 3h. Cells were fixed with fresh 4 % paraformaldehyde solution for 15 min at room temperature. Next, cells were permeabilized with 1 % Triton X (Sigma, St Louis, MO) for 15min on ice, followed by incubation in 10 % normal goat serum blocking solution (Zymed Laboratories, Carlsbad, CA, USA) for 20 min at room temperature in a humidified chamber. We determined the interaction between the FGFR4 and P62 proteins using the Duolink *In Situ* Proximity Ligation Assay (PLA) Detection Kit (Sigma-Aldrich), and the immunofluorescence was performed following supplier's instructions. Briefly, cells were incubated with a combination of two antibodies, one from mouse and one from rabbit donors diluted in antibody diluent solution (1:100) overnight at 4 °C. Next day, the primary antibodies were removed from the chamber slide. The slide was washed once, and secondary antibodies conjugated with oligonucleotides (Duolink In Situ PLA Probe Anti-Mouse Minus and Duolink In Situ PLA Probe Anti Rabbit Plus; Sigma-Aldrich) were added and incubated in a preheated humidity chamber for 1h at 37 °C. The probes were removed, and the slide was washed twice for 5 min under gentle agitation. The ligation–ligase solution was added to each sample and incubated in a preheated humidity chamber for 30 min at 37 °C. For amplification, the slides were washed twice for 2 min and the amplification polymerase solution was added and incubated for 100 min in a preheated humidity chamber at 37 °C. Finally, the slides were washed, dried, and an In Situ Mounting Medium with DAPI (Sigma) was applied. Non-specific signals were assessed by using single primary antibody staining for P62 or FGFR4, or no antibody, as a control. The fluorescence signal was detected using Keyence BZX-700 microscopy.

2.11. Immunoprecipitation

MKN28 cells were washed with cold PBS, scraped and resuspended in 1 ml of cell lysis buffer from the MCL1–1 KT Mammalian Cell Lysis Kit (Sigma-Aldrich, Milwaukee, WI). Cells were rocked for 15 min at 4 °C, followed by sonication for 10 s for a total of 3 times. The lysates were centrifuged for 10 min at 12,000g at 4 °C. Immunoprecipitation was performed using Dynabeads Protein G (Dynal, Invitrogen Life Sciences, Carlsbad, CA) according to the manufacturer's instructions. FGFR4 or P62, or KEAP1 antibody (Santa Cruz Biotechnology) was cross-linked to Dynabeads Protein G. The cell lysates were added to the cross-linked beads and incubated for 2 h with rocking. The Dynabeads were then pelleted using a magnet and washed three times with a washing buffer. The captured protein was eluted from beads by adding 40 μl of 2 × protein-loading buffer to each sample and boiling for 10 min. Samples were resolved by SDS/PAGE and subjected to western blotting.

2.12. Spheroid culture

MKN28 cells transfected with FGFR4 or control siRNA were infected with *H. pylori*, seeded into ultra-low attachment 24-well dishes (Corning, Corning, NY) in serum-free DMEM/F12 supplemented with 20 ng/mL epidermal growth factor (EGF), 2 % B-27 (Life Technologies, Carlsbad, CA) and 10 ng/mL basic fibroblast growth factor (bFGF). After four days, three random 4× magnification fields were captured using the bright field mode Microscope (BZ-X700, Keyence Corp, Atlanta, GA). The size and number of tumor spheres in each field were calculated using ImageJ software.

2.13. Immunohistochemistry on tissue microarray and quantification

Immunohistochemical (IHC) analysis of FGFR4 and NRF2 protein expression was performed on a tissue microarray (TMA) that contained 63 adenocarcinomas, 9 high grade dysplasia, 20 intestinal metaplasia (IM) and 20 normal gastric samples. All coded tissue samples were histologically verified, and representative regions were selected for inclusion in the TMA. 5 μm sections were prepared, deparaffinized and dehydrated using xylene and decreasing serial dilutions of ethanol. TMA slide sections were immersed in boiling 1xTris-EDTA (pH = 9) for 30 min for antigen unmasking. After washing with water, tissue sections were incubated in H_2O_2 for 10 min and then blocked with goat serum for 20 min at room temperature. After washing, sections were incubated overnight at 4 °C with the primary antibody against FGFR4 (1:1000) ProteinTech, NRF2 (1:1000) Abcam or P62 (1:2000) Cell Signaling. The next day, slides were incubated with secondary antibodies using IHC Select Immunoperoxidase Secondary Detection System (Millipore, DAB150) following the manufacturer's instructions. TMA slides were counterstained with Hematoxylin and mounted with a xylene-based mounting medium. Images were visualized using Olympus BX51 bright field microscope (Olympus Co). For quantification, the Immunohistochemical results were calculated for intensity and frequency of staining. The intensity of staining was classified as 0 (negative), 1 (weak), 2 (moderate) and 3 (strong). The frequency was arranged from 0 to 4 by a percentage of positive cells as follows: grade 0, <3 %; grade 1, 3–25 %; grade 2, 25–50 %; grade 3, 50–75 %; grade 4, more than 75 %. Thecomposite index score was the product of multiplying the intensity and frequency grades with a range from 0 to 12.

2.14. Public dataset analysis

To determine the optimal cutoff points of FGFR4 mRNA expression, we used R software, and the values above or below the median ± SD were defined as "High" or "Low," respectively. The FGFR4 and P62 gene expression levels were analyzed in normal and stomach adenocarcinoma tissue samples using the TNMplot online tool (https://tnmplot.com/analysis/) [25]. The RNA-Seq data were extracted from the Gene Expression Omnibus of the National Center for Biotechnology Information (CBI-GEO) for 294 normal gastric tissue samples and 375 gastric adenocarcinoma tissues.

Additional information about reagents and antibodies are listed in Supplemental Tables 2 and 3, respectively.

3. Results

3.1. High expression levels of FGFR4 are associated with decreased gastric cancer patients' survival

Using the open data source from the TNM plotter database (https://tnmplot.com/), the RNA seq data showed that FGFR4 is significantly overexpressed in human stomach adenocarcinomas (n = 375), as compared to normal samples (n = 294) (Supplemental Fig. 1A). Kaplan-Meier survival plot analysis in gastric cancer patients with high FGFR4 expression (n = 302) showed lower survival rates as compared to patients with low FGFR4 (n = 574) (Supplemental Fig. 1B).

3.2. FGFR4 expression is associated with oxidative stress signature

Analysis of TCGA data as well as eight additional public GEO databases (GSE66229, GSE15459, GSE26901, GSE13861, GSE110875, GSE34942, GSE100935 and GSE30727), showed oxidative phosphorylation signature among the top 13 molecular functions associated with overexpression of FGFR4, as demonstrated by the Ridge plot (Fig. 1A, Supplemental Table 4). GSEA analysis from the TCGA cohort confirmed the enrichment for oxidative phosphorylation and reactive oxygen species (ROS) response genes in FGFR4-high samples (Fig. 1B, Supplemental Table 5). These results suggested a link between FGFR4 levels and ROS. *H. pylori* infection generates high ROS levels resulting in damage to gastric mucosa [6,26]. Gastric cells must develop molecular mechanisms to control and maintain ROS below lethal levels. We investigated whether FGFR4 plays a role in regulating infection-induced ROS. The siRNA knockdown of FGFR4 in MKN28 and AGS cells demonstrated higher levels of intracellular ROS in response to *H. pylori* infection, as measured by CM-H2DCFDA fluorescent intensity, as compared to siRNA controls (Fig. 1C&D and Supplemental Fig. 2A&B). These results were confirmed by 8-oxoguanine staining, a marker for oxidative DNA damage. The siRNA knockdown of FGFR4 in MKN28 and AGS cells demonstrated higher 8-oxoguanine immunostaining levels, a marker of oxidative DNA damage, in response to *H. pylori* infection (Fig. 1E&F and Supplemental Fig. 2C&D). These data indicate that FGFR4 played a role in protecting epithelial cells by decreasing the *H. pylori*-mediated spike in ROS levels.

3.3. FGFR4 regulates NRF2 protein levels and transcription activity

Because NRF2 is known as the master antioxidant transcription factor, we hypothesized that FGFR4 regulates ROS levels via NRF2 activation. We also hypothesized that induction of FGFR4-NRF2 would be dependent on the ROS generated by infection, as a cellular protective response mechanism to prevent toxic increase in ROS levels. Using ROS scavenger (N-acetyl-L-cysteine "NAC"), we first checked the levels of FGFR4 and NRF2 in *H. pylori* infected cell lines. MKN28 cells were treated overnight with NAC (200 μM) and infected with J166 and 7.13 *H. pylori* strains for 3 h next day. Western blot analysis showed that after infection with *H. pylori*, the FGFR4 and NRF2 protein levels were decreased in NAC treated cells as compared to non-treated cells (Supplemental Fig. 3A and B). These data indicate that induction of FGFR4 and NRF2 was dependent on the ROS levels generated by *H. pylori* infection. Next, we investigated human samples in public data sets to determine the correlation between *FGFR4* mRNA level and single-sample gene set enrichment analysis (ssGSEA) score for NRF2 gene set signature in TCGA gastric cancer cohort. Using Pearson's correlation analyses, the data showed a positive correlation between NRF2 ssGSEA score and FGFR4 mRNA expression in gastric cancer (Fig. 2A). Next, we performed GSEA of NRF2 signature using the TCGA dataset (Supplemental Table 6). This analysis indicated that NRF2 signature was significantly enriched in $FGFR4^{high}$ compared with $FGFR4^{low}$ gastric tissue samples (p = 0.002) (Fig. 2B, Supplemental Fig. 3C&3D). To confirm the bioinformatics data, we transfected MKN28 and AGS gastric cancer cell lines with different doses of FGFR4 expression vector and showed an increase in NRF2 protein level after overexpression of FGFR4 (Supplemental Fig. 3E&F). The knockdown of endogenously high levels of FGFR4 in MKN45 cells demonstrated opposite results, with an almost complete loss of NRF2 (Supplemental Fig. 3G). Using the TFF1-KO mouse model of chronic inflammation and gastric neoplasia similar to human [20,27], we demonstrated high levels of FGFR4 with NRF2 nuclear accumulation and localization in the antro-pyloric dysplastic regions of the stomach (Fig. 2C). Western blot analysis showed high FGFR4, p-FGFR4 (Y642), NRF2 and HO1 protein levels in the TFF1-KO mice gastric tissues compared to control mice (Fig. 2D). Additionally, we

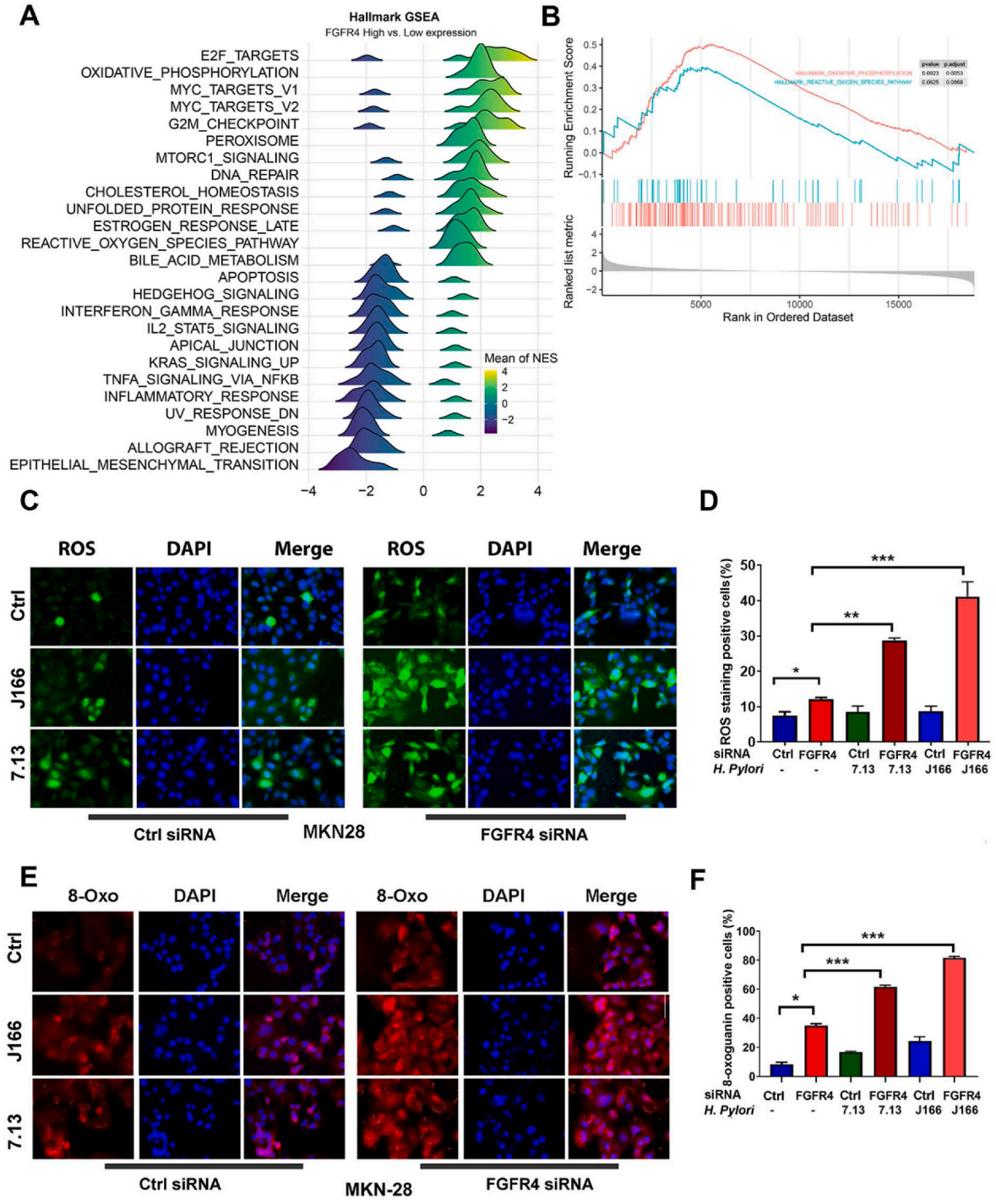

Fig. 1. High FGFR4 expression is associated with the oxidative stress pathway in gastric cancer. A) The Ridge plot by Gene set enrichment analysis (GSEA) was performed using *FGFR4*^{high} expression samples, compared with *FGFR4*^{low} expression samples in the TCGA and eight GEO databases (GSE66229, GSE15459, GSE26901, GSE13861, GSE110875, GSE34942, GSE100935 and GSE30727).Hallmark gene sets were downloaded from MSigDB (https://www.gsea-msigdb.org/). B) Oxidative phosphorylation gene set and reactive oxygen species pathway were significantly enriched in high *FGFR4* expression samples in the TCGA cohort. C) Representative images of CM-H2DCFDA immunofluorescent staining showing higher ROS levels in MKN28 cells infected with *H. pylori* J166 or 7.13 strains (3h). ROS levels were significantly increased following FGFR4 knockdown. D) Quantification of CM-H2DCFDA positive staining in at least two hundred cells from three images is presented as a percentage in the right panel. Data are graphed with mean ± SEM. E) Immunofluorescence staining of 8-oxoguanine demonstrates a significant increase in oxidative DNA damage after infection with *H. pylori.* This increase was significantly enhanced following FGFR4 knockdown. F) quantification of 8-oxo-guanine immunofluorescent staining as in D. Data are graphed with mean ± SEM. $*P < 0.05$, $**P < 0.01$, $***P < 0.001$.

assessed the mRNA expression of *Fgfr4, Fgf15* (the mouse ortholog for human *FGF19*) and *Ho1* genes in the gastric tissue of TFF1-KO and TFF1-WT mice. The RT-qPCR data revealed a significant increase in the mRNA expression levels of all the genes mentioned above in TFF1-KO mice as compared to TFF1-WT mice (Fig. 2E). Taken together, these results confirmed the role of FGFR4 in mediating an increase in NRF2 protein levels with nuclear accumulation and upregulation of oxidative stress genes in gastric tumors.

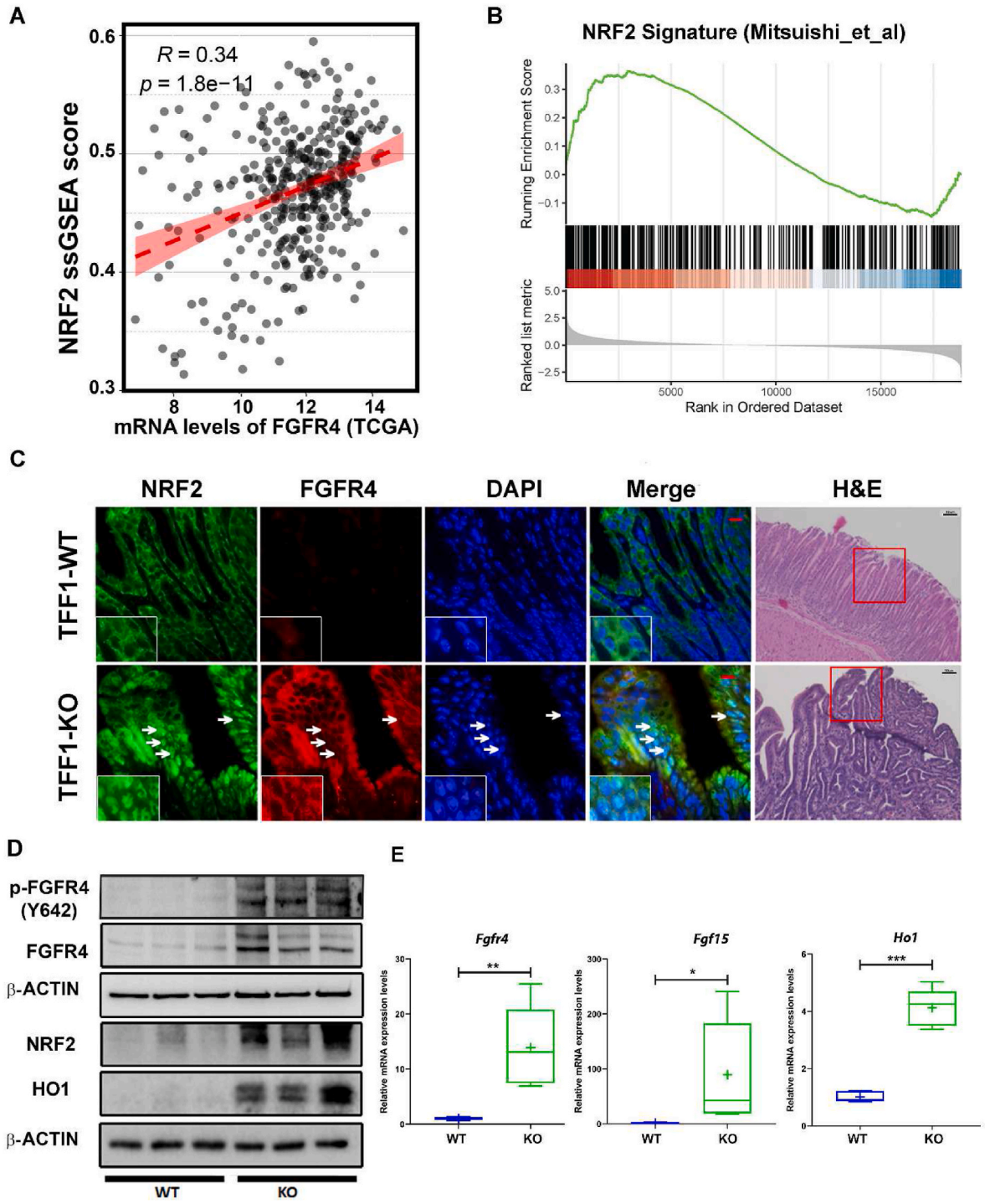

Fig. 2. Positive correlation between FGFR4 and NRF2 in gastric cancer. A) Pearson's correlation analysis between *FGFR4* mRNA level and single-sample gene set enrichment analysis (ssGSEA) scores for NRF2 targets' signature in the TCGA cohort. B) GSEA was performed using samples with *FGFR4*^{high} expression compared to samples with *FGFR4*^{low} expression in TCGA cohort. NRF2 signature [49] was significantly enriched in *FGFR4*^{high} expression samples. C) Immunofluorescence analysis shows an increase of NRF2 nuclear staining (green) and FGFR4 expression (red) in TFF1-KO mouse neoplastic gastric tissues, as compared to normal gastric tissues from the TFF1-WT mice (scale of 10 μm is shown in the merged image). The arrows point to nuclei. The right panels show bright field image of H&E staining. D) Western blot analysis demonstrates an increase of p-FGFR4 (Y642), FGFR4, NRF2 and HO1 protein levels in neoplastic gastric tissues (KO), as compared to normal tissue samples (WT) from mice. RT-qPCR analysis of *Fgfr4, Fgf15 and Ho1* mRNA expression in gastric tissues of TFF1-KO mouse as compared to TFF1-WT. $*P < 0.05$, $**P < 0.01$ and $***P < 0.001$ is considered significant. (For interpretation of the references to colour in this figure legend, the reader is referred to the Web version of this article.)

3.4. *H. pylori* infection induces FGFR4-dependent increase in NRF2

We investigated if FGFR4 was required for the induction of NRF2 in response to *H. pylori* infection conditions in MKN28 and AGS cells (AGS data are shown in supplementary figures). Western blot analysis confirmed these findings, showing an FGFR-dependent increase in NRF2 and its classical target HO1. These effects were lost in conditions of FGFR4 knockdown (Fig. 3A and Supplementary Fig. 4A).

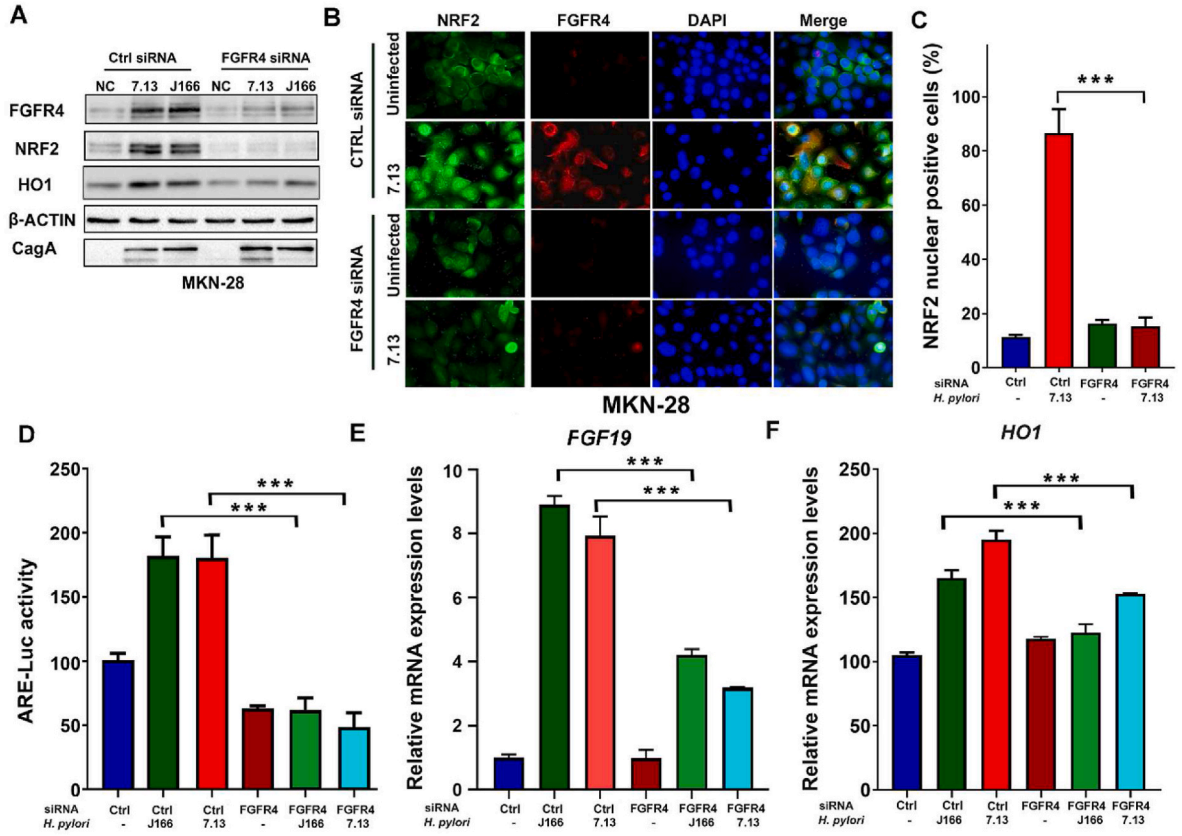

Fig. 3. FGFR4 knockdown reduces NRF2 protein and transcription activity levels. A) Western blot shows an increase of FGFR4, NRF2 and HO1 proteins after *H. pylori* infection (3h) as compared to uninfected negative control (NC). FGFR4 siRNA knockdown abrogated this increase. B) Immunofluorescence assay demonstrates an increase of NRF2 nuclear staining in *H. pylori* Infected cells. This increase was abolished with FGFR4 siRNA knockdown. C) Quantification of nuclear NRF2-positive staining in at least 200 cells from three images is presented as a percentage in the right panel. Data are graphed with mean ± SEM. D) The NRF2 transcriptional activity was measured by the ARE luciferase reporter assay following infection with *H. pylori* in MKN28 cells. *H. pylori* induced the activity of the reporter, whereas FGFR4 siRNA knockdown reversed this effect. The luciferase reporter activity values were normalized to β-gal expression levels and are represented as luciferase activity relative to control. E-F) RT-qPCR of *FGF19* (E) and *HO1* (F) following infection with *H. pylori* (3h) in MKN28 cells transfected with control siRNA or FGFR4 siRNA. ***$P < 0.001$.

Immunofluorescence analysis confirmed these findings and showed an increase of FGFR4 staining along with nuclear localization of NRF2 in *H. pylori* infected MKN28 and AGS cells; this increase was abolished after FGFR4 silencing (Fig. 3B&C, Supplemental Fig. 4B&C). By measuring the NRF2 transcription activity, using the ARE luciferase reporter assay, we detected an increase in the reporter activity following infection with J166 and 7.13 *H. pylori* strains, an effect that was abrogated upon FGFR4 knockdown (Fig. 3D and Supplementary Fig. 4D). Using RT-qPCR analysis, we observed a significant increase in *FGF19 and HO1* mRNA expression in J166 and 7.13 *H. pylori* infected cells (Fig. 3E and F). This increase was notably reduced after FGFR4 knockdown (Fig. 3E and F). Of note, there was no significant difference in the mRNA expression levels of NRF2 under these conditions, ruling out transcription regulation of NRF2 by FGFR4 (Supplemental Fig. 4E&F). Using western blots, we analyzed the levels of FGFR4, NRF2 and HO1 in response to stimulation with FGF19, an FGFR4 ligand in gastric cells [15]. As expected, the FGFR4 protein level was increased following FGF19 treatment, promoting an increase in NRF2 and HO1. The knockdown of FGFR4 markedly decreased these FGF19-mediated changes (Supplemental Fig. 5A&B). Similar effects were noted in non-neoplastic GES1 gastric cells (Supplemental Fig. 5C). To confirm these data, we established normal human gastric organoids transfected with FGFR4 or control short hairpin RNA treated or not with FGF19 recombinant protein for 24h. The control organoids showed increased FGFR4 and nuclear NRF2 protein staining with FGF19 stimulation (Supplementary Fig. 5D). However, NRF2 nuclear staining was absent in organoids with FGFR4 knockdown (Supplementary Fig. 5D). Collectively, these data confirm the role of FGFR4 in the induction and activation of NRF2.

3.5. *H. pylori* infection induces FGFR4 and NRF2 in vivo

To validate the *in vitro* data, we utilized mouse models for infection using the mouse-adapted PMSS1 strain of *H. pylori*. Immunofluorescence analysis of the antro-pyloric glandular stomach tissues, collected after 4-weeks of infection, showed an increase in FGFR4 with accumulation and nuclear localization of NRF2, compared to non-infected mice (Fig. 4A). To confirm the immunofluorescence results, we determined the protein levels of FGFR4, p-FGFR4 (Y642), NRF2 and HO1 using western blot analysis. The results demonstrated an increase in FGFR4, NRF2 and HO1 protein levels following *H. pylori* infection, as compared to controls (Fig. 4B). Next, we checked the mRNA expression of *Fgfr4, Ho1,* and *Fgf15* genes in the gastric tissue of infected and non-infected mice. The RT-qPCR data demonstrated a significant increase in the mRNA expression levels of all genes mentioned above in gastric tissues infected with the PMSS1 *H. pylori* strain (Fig. 4C).

3.6. Inhibition of FGFR4 decreased NRF2 protein level and activity in vitro and in vivo

The use of H3B-6527, a potent and selective inhibitor of FGFR4 [28, 29], abrogated the *H. pylori* mediated increase in NRF2 protein level (Fig. 5A) and transcription activity (Fig. 5B), as measured by the ARE

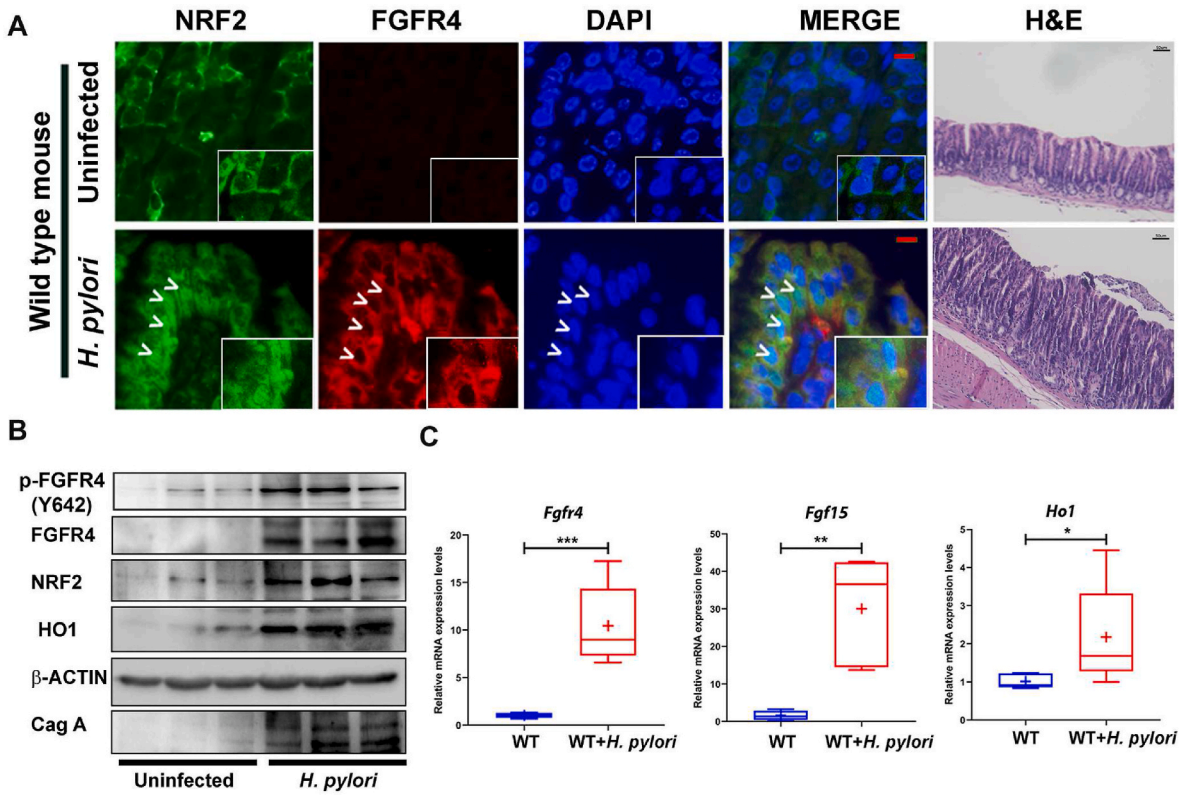

Fig. 4. NRF2 nuclear expression is associated with *H. pylori* infection and tumorigenesis in mouse gastric tissues. A) Immunofluorescence analysis shows an increase of NRF2 (green) nuclear staining (arrow heads) and FGFR4 expression (red; arrow heads) in wild-type mice (C57/B6) gastric tissues after *H. pylori (*PMSS1 strain*)* infection for four weeks (scale of 10 μm is shown in the merged image). The right panels show bright field images of H&E staining. The arrowheads point to the nuclei. B) Western blot analysis demonstrates an increase in the protein levels of p-FGFR4 (Y642), FGFR4, NRF2 and HO1 in gastric tissues of mice infected with PMSS1 as compared to uninfected mice. C) RT-qPCR analysis of *Fgfr4, Fgf15 and Ho1* mRNA expression in gastric tissues of mice infected with PMSS1 as compared to uninfected mice. $*P < 0.05$, $**P < 0.01$, $***P < 0.001$. (For interpretation of the references to colour in this figure legend, the reader is referred to the Web version of this article.)

luciferase reporter. To confirm the *in vitro* data, we used three groups of wild-type mice. Two groups were infected with *H. pylori* PMSS1 for 4 weeks, and one group was used as noninfected control. After 4 weeks, one group of the infected mice was given H3B-6527 (300 mg/kg) by oral gavage for 4 consecutive days. The immunofluorescence data analysis showed an increase of FGFR4 and nuclear localization of NRF2 staining in the antro-pyloric region of mice gastric tissues after infection with PMSS1 (Fig. 5C). This increase was completely abolished after treatment with H3B-6527 (Fig. 5C). Western blot analysis confirmed the immunofluorescence data and showed an increase of FGFR4, p-FGFR4 (Y642) and NRF2 protein levels in the PMSS1-infected mice, compared with control uninfected mice (Fig. 5D). In addition, the RT-qPCR data demonstrated a significant increase in the mRNA expression levels of *Fgfr4* and *Ho1* after *H. pylori* infection, as expected; this increase was abolished after treatment with H3B-6527 (Fig. 5E). Taken together, these results confirm an FGFR4-dependent regulation of NRF2 in gastric cells *in vitro* and *in vivo*.

3.7. FGFR4 overexpression correlates with an increase in P62 level

KEAP1, an adapter subunit of CUL3 E3 ubiquitin ligase, mediates ubiquitination and degradation of NRF2 under normal physiological conditions. This physiological regulatory mechanism is largely disrupted in cancer cells. Previous studies have shown that aberrant NRF2 accumulation in cancer cells [30,31] can be through disruption of the binding of KEAP1 to NRF2 [32]. The P62, also called SQSTM1, can interact with KEAP1 and compete with NRF2 binding, leading to NRF2 accumulation and activation [33]. Of note, we did not detect changes in KEAP1 levels under our experimental conditions in both MKN28 and AGS cell lines (Supplementary Fig. 6A&B). Using the TNM plotter database, we investigated the expression of *P62* in 375 human gastric adenocarcinomas samples as compared to 294 normal human gastric samples. We found a significant increase in *P62* gene expression in patients with gastric adenocarcinoma compared to normal (Supplemental Fig. 7A). High expression levels of *P62* correlated with poor overall survival in gastric cancer patients, as estimated by Kaplan Meier curve (Supplemental Fig. 7B). We also detected a significant positive correlation between *P62* and *FGFR4* (Supplementary Fig. 7C. $P < 0.001$). Gastric cancer patients with $P62^{high}$ $FGFR4^{high}$ tumors had worse overall survival, as compared with patients with $P62^{low}$ $FGFR4^{low}$ tumors (Supplementary Fig. 7D. $P < 0.001$).

We examined the levels of P62 in three different cell lines (MKN28, AGS and GES1) infected with *H. pylori* or stimulated with FGF19 recombinant protein after FGFR4 knockdown. Western blot analysis demonstrated an increase in the protein levels of P62, p-P62 (S349), FGFR4, and p-FGFR4 (Y642), as well as NRF2, following *H. pylori* infection (Fig. 6A and Supplementary Fig. 8A&C). This increase was significantly reversed after FGFR4 knockdown (Fig. 6A and Supplementary Fig. 8A&8C). Similar results were obtained with FGF19 recombinant protein stimulation (100 ng/ml) (Fig. 6B and Supplementary Fig. 8B&8D). Next, we investigated if FGFR4 regulates NRF2 protein stability. We performed cycloheximide (CHX) chase assay in MKN28 cells with and without FGFR4 silencing after *H. pylori* infection. Western blot analysis indicated that NRF2 protein was more rapidly degraded after FGFR4 siRNA knockdown with half-life t(1/2) = 25min, as compared to half-life t(1/2) = 61min in siRNA control cells (Fig. 6C). Using P62 siRNA, we detected similar results, and NRF2 protein was degraded faster (half-life t(1/2) = 25min), as compared to control cells

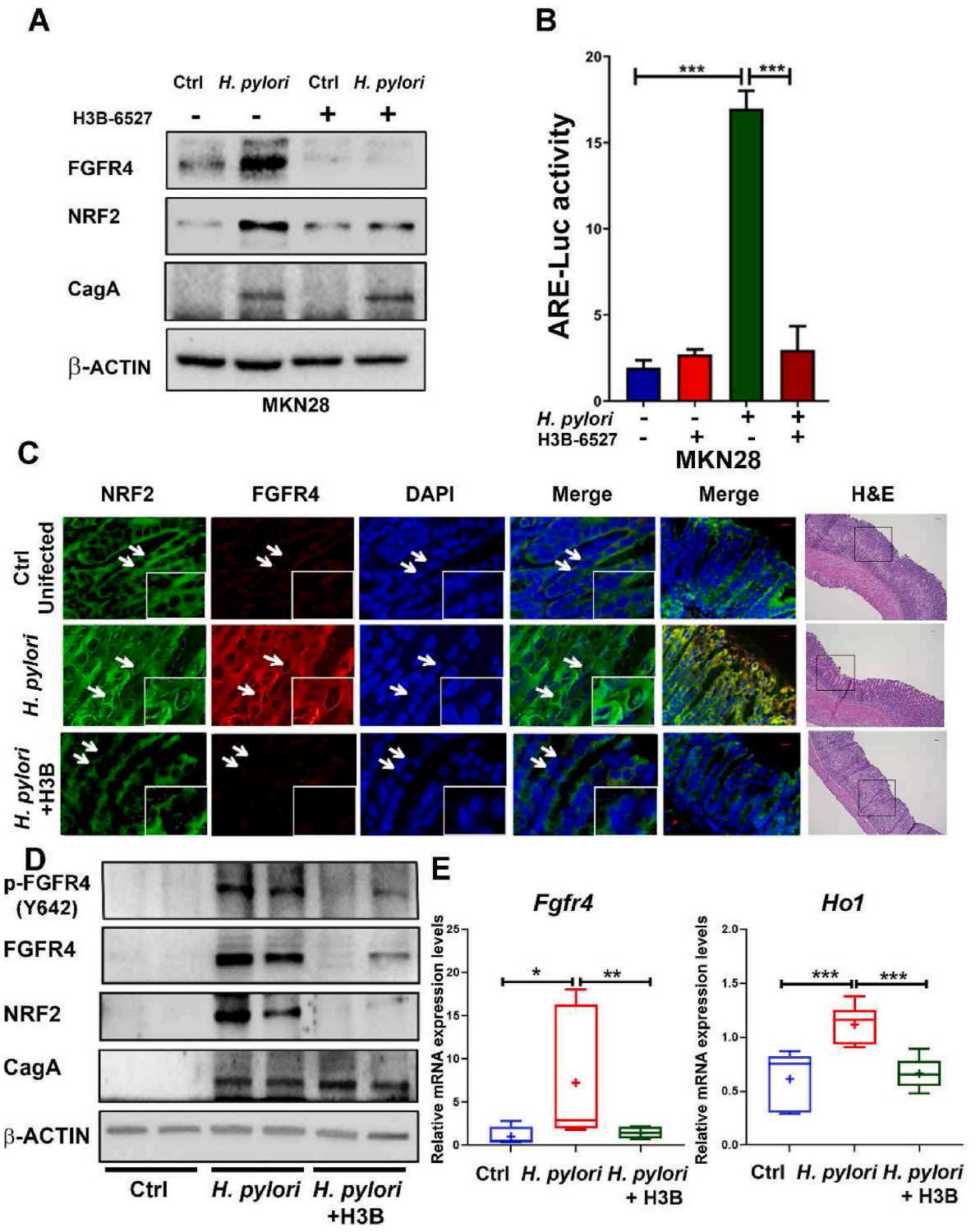

Fig. 5. FGFR4 inhibition decreases NRF2 *in vitro* and *in vivo*. A) Western blot analysis in MKN28 cells. Treatment with FGFR4 inhibitor (H3B-6527) abrogates *H. pylori* (7.13)-mediated increase in NRF2. B) The ARE luciferase reporter assay was used as a measure of NRF2 transcriptional activity under similar conditions as in B, demonstrating a significant induction of luciferase activity by *H. pylori* (7.13) infection, an effect that was abolished with the H3B-6527 inhibitor. The luciferase reporter activity values were normalized to β-gal expression levels and are represented as luciferase activity relative to control. C) Immunofluorescence analysis shows an increase of NRF2 (green) nuclear staining and FGFR4 expression (red) in wild-type mice (C57/B6) gastric tissues after four weeks of infection with *H. pylori* (PMSS1); nuclear localization of NRF2 was abolished after treatment with H3B-6527 (H3B); arrows point to nuclei. The right panels show bright field images of H&E staining. D) Western blot analysis of mouse gastric tissues shows an increase of p-FGFR4 (Y642), FGFR4 and NRF2 in infected mice; this increase was abolished after treatment with H3B-6527. E) RT-qPCR analysis of *Fgfr4 and Ho1* mRNA expression in gastric tissues of mice infected with PMSS1 and treated or not with H3B-6527 (H3B) and compared to uninfected mice. *$P < 0.05$, **$P < 0.01$, ***$P < 0.001$. (For interpretation of the references to colour in this figure legend, the reader is referred to the Web version of this article.)

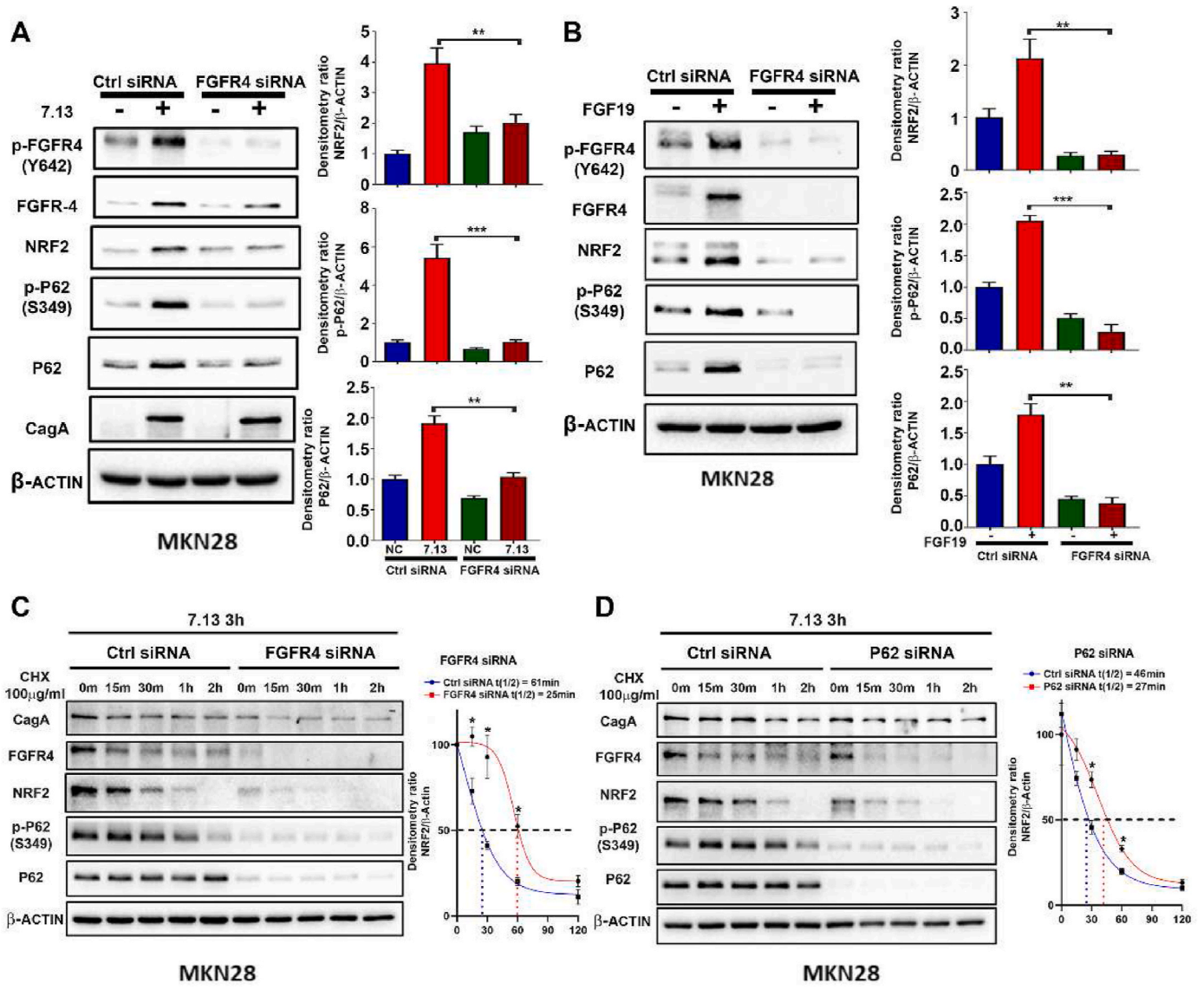

Fig. 6. FGFR4 induces P62 to promote NRF2 protein stability. A) Western blot analysis using MKN28 cells uninfected or infected with *H. pylori (7.13, 3h)*. Infected cells show high levels of p-FGFR4 (Y642), FGFR4, NRF2, p-P62 (S349) and P62. These changes were reversed upon FGFR4 siRNA knockdown. The relative intensity ratios of NRF2/β-Actin, p-P62/β-Actin, and P62/β-Actin were calculated by ImageJ software and shown on the right panel. The results are expressed as mean ± SEM of at least three independent experiments. B) Western blot analysis following treatment of MKN28 cells with FGF19 (30 min). This stimulation led to increases in p-FGFR4 (Y642), FGFR4, NRF2, p-P62 (S349) and P62. These changes were reversed with FGFR4 siRNA knockdown. The Bar graphs show the relative intensity ratios of NRF2/β-Actin, p-P62/β-Actin, and P62/β-Actin were calculated and shown on the right panel. The results are expressed as mean ± SEM of at least three independent experiments. C-D) Western blot showing cycloheximide chase assay of NRF2 using FGFR4 siRNA (C) or P62 siRNA (D) at the indicated time points, following *H. pylori* infection (3h). NRF2 protein stability was reduced following FGFR4 or P62 knockdown. The half-life time (t1/2) of NRF2 was calculated using GraphPad Prism software and plotted on the right side of panels C and D, respectively. *P < 0.05, **P < 0.001.

with half-life t(1/2) = 46min (Fig. 6D). Taken together, these data indicated that FGFR4 promoted NRF2 protein stability, similar to P62.

3.8. FGFR4 regulates NRF2 stability via binding to KEAP1 and P62

It was reported that P62 could interact with the NRF2-binding site on KEAP1, a component of Cullin-3-type ubiquitin ligase for NRF2, promoting NRF2 stability [33]. We confirmed the competitive interaction of NRF2 and P62 to KEAP1 by performing a KEAP1 immunoprecipitation and P62 knockdown in conditions of *H. pylori* infection. The results demonstrated an increase in the interaction of NRF2 and KEAP1 after P62 knockdown (Supplemental Fig. 9). We next investigated whether FGFR4 can be part of the P62-KEAP1 complex, protecting NRF2 and allowing its accumulation. We performed a P62 immunoprecipitation assay followed by immunoblot analysis of FGFR4, NRF2 and KEAP1, in conditions of FGFR4 knockdown, or control, with or without *H. pylori* infection. The results demonstrated a novel protein interaction between FGFR4, P62 and KEAP1 in the control cells following *H. pylori* infection. The P62-KEAP1 interaction was abolished after FGFR4 siRNA knockdown (Fig. 7A). Next, we determined the interacting proteins with and without P62 knockdown. FGFR4 pulldown confirmed the interaction between FGFR4, P62, and KEAP1 in control cells, following *H. pylori* infection. This interaction between FGFR4 and KEAP1 was suppressed after the knockdown of P62 (Fig. 7B). We did not detect a significant interaction between NRF2 and FGFR4 or P62; however, there was an increase in the interaction of NRF2 and KEAP1 after P62 knockdown (Supplemental Fig. 9). The proximity ligation assay results confirmed the proximity of P62 to FGFR4 in control cells infected with *H. pylori* (Fig. 7C), in agreement with the findings from immunoprecipitation. As a negative control, the proximity ligation assays were performed with

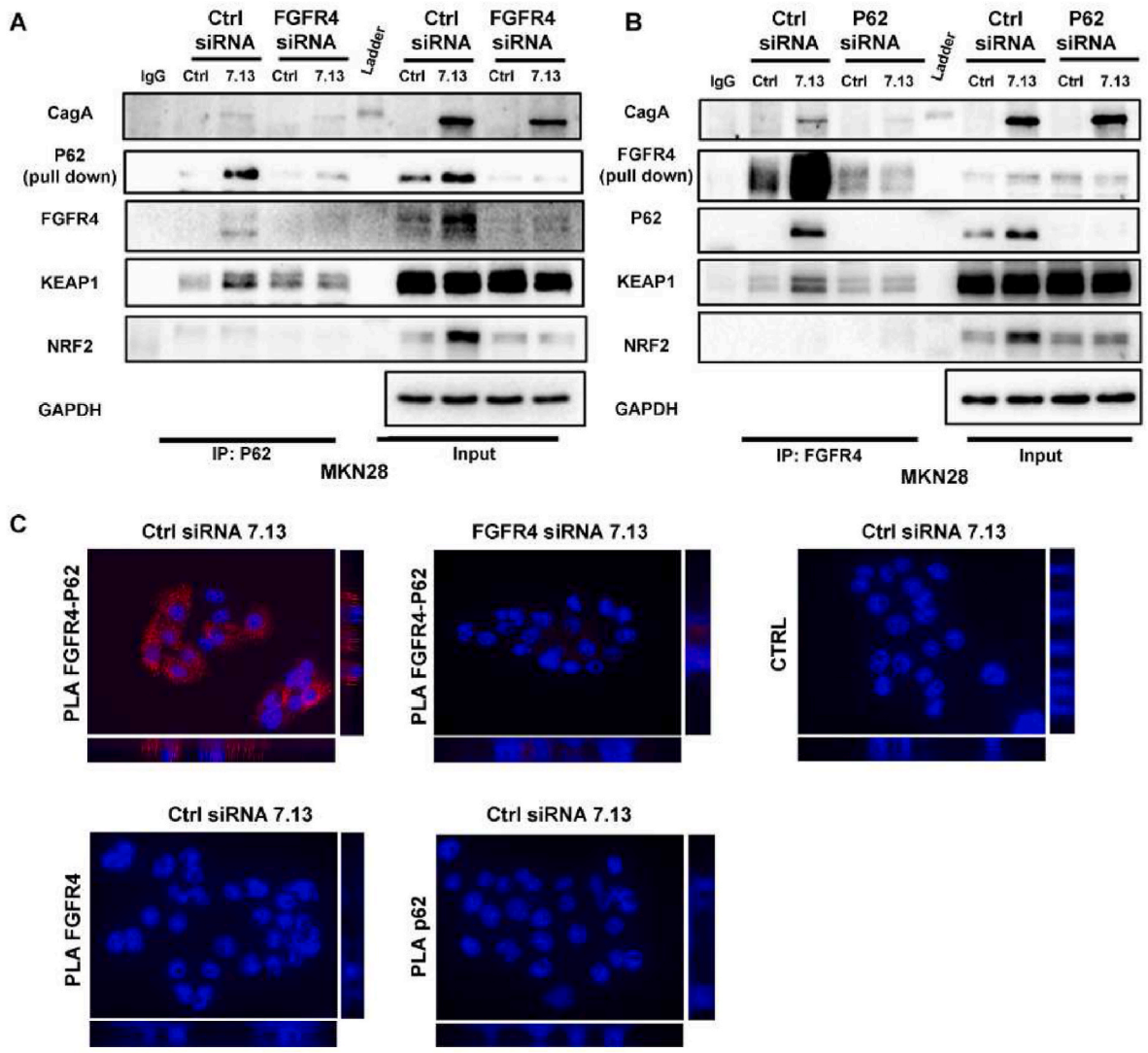

Fig. 7. FGFR4, P62, and KEAP1 coexist in the same protein complex. A-B) Immunoprecipitation and western blot analysis following P62 pulldown (A) or FGFR4 pulldown (B) using MKN28 cells infected with *H. pylori* 7.13 (3 h). Immunoprecipitations and their corresponding input samples were subjected to immunoblotting with P62 FGFR4 Keap1 and NRF2 antibodies. The infection was confirmed using CagA antibody and equal amounts of protein loading were confirmed in the input samples using GAPDH antibody. C) Proximity ligation assay was performed in MKN28 cells transfected with control or FGFR4 siRNA and infected with *H. pylori (*7.13). The presence of red signals indicates positive ligation and proximity of the proteins, indicative of interaction. Using FGFR4 and P62 antibodies, the results indicated the presence of FGFR4-P62 interaction (red signals) following *H. pylori* infection (left upper panel). This interaction was not detected with FGFR4 siRNA (middle upper panel). The lower panels display the negative control for PLA background reaction. Control cells were transfected with Ctrl siRNA, infected with *H. pylori* and probed with a single antibody against FGFR4 (lower left panel) or P62 (lower right panel). The upper right panel displays a negative control for the PLA background with no antibody. Maximum intensity projection is presented on the right and lower sides of each image. (For interpretation of the references to colour in this figure legend, the reader is referred to the Web version of this article.)

single and no antibodies (Fig. 7C). Our results indicate that FGFR4-P62-KEAP1 interaction interferes with NRF2 binding to KEAP1/CUL3 degradation complex, thus allowing NRF2 accumulation.

3.9. FGFR4 promotes spheroids' cellular expansion after H. pylori infection

To investigate the role of FGFR4 in promoting cellular plasticity and survival, we examined spheroid's growth under conditions of *H. pylori* infection with and without FGFR4 knockdown, compared to controls. We detected a significant increase in the size (Fig. 8A and B) and number of spheres after *H. pylori* infection (Fig. 8C); this increase was significantly reduced after FGFR4 knockdown. Western blot analysis of spheroids confirmed our previous findings and showed an increase in FGFR4, NRF2, and P62 protein levels after *H. pylori* infection (Fig. 8D). This increase was decreased after FGFR4 knockdown (Fig. 8D).

3.10. Overexpression of FGFR4, P62, and NRF2 in human gastric cancer tissues

We next investigated the expression of FGFR4, NRF2 and P62 protein on coded human tissue samples, using immunohistochemistry analysis on gastric cancer TMA samples (20 normal, 9 High grade dysplasia and 63 gastric adenocarcinomas) (Fig. 8E, Supplemental Fig. 10A). Utilizing the composite expression score (CES). The IHC analysis of FGFR4, NRF2, and P62 protein expression showed higher immunostaining levels in tumors (score 7-12) for FGFR4 (Figs. 8F, 51 %), NRF2 (Figs. 8G, 68 %) and P62 (Supplemental Fig. 10B, 42 %) in gastric adenocarcinoma. We also used the Cochran-Mantel-Haenszel Statistical analysis method to analyze the IHC expression scores across histological stages. The results

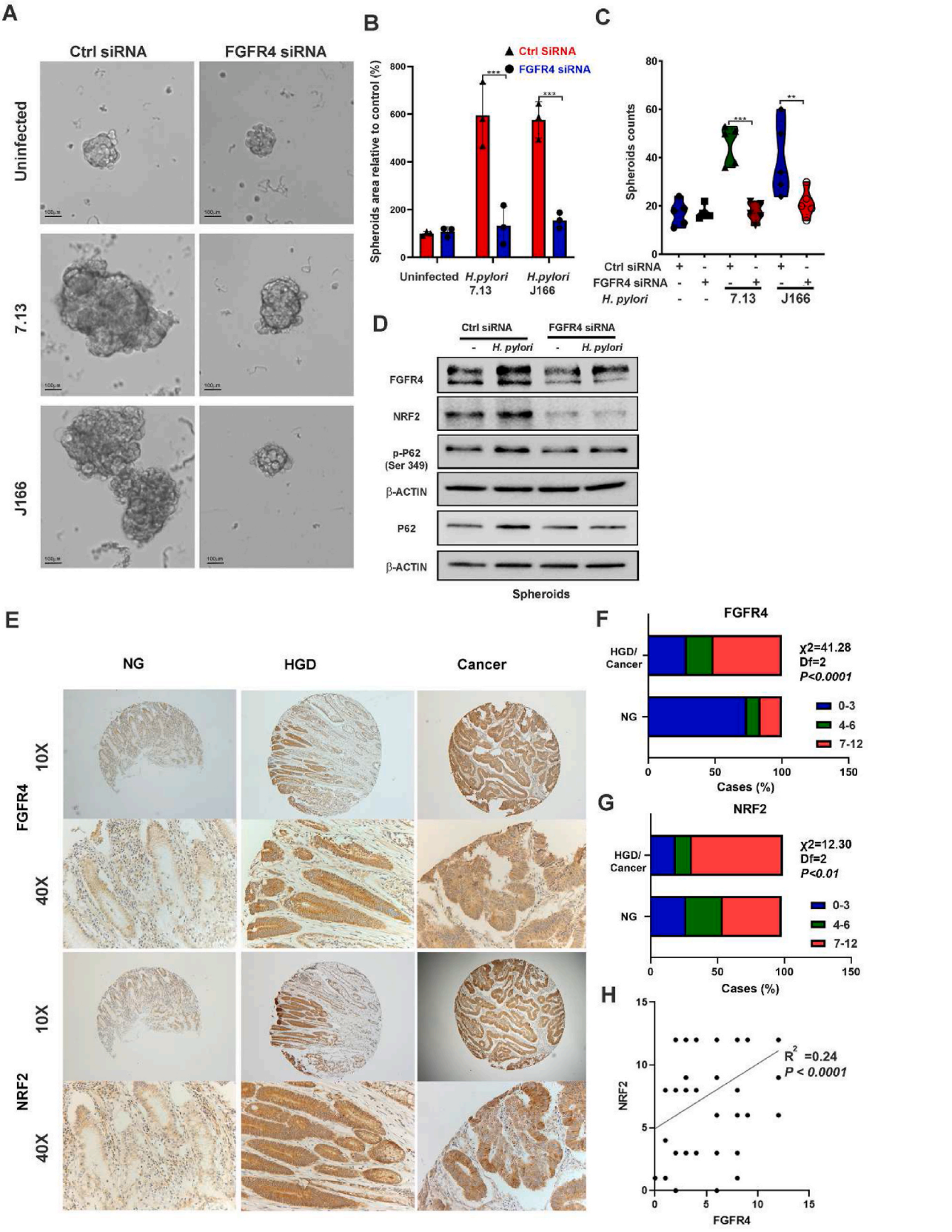

(caption on next page)

Fig. 8. FGFR4 promotes cell expansion and correlates with NRF2 in gastric cancer. A) Representative images of spheroids showing an increase in size and number of spheroids after *H. pylori* infection, an effect that was abrogated upon FGFR4 knockdown (scale 100 μm). B & C) Quantification of the size of at least twenty spheroids (B) and sphere counts (C) from three different fields. D) Western blot analysis using spheroids derived from MKN28 cells uninfected or infected with *H. pylori* (7.13). Infected cells show higher levels of FGFR4, NRF2, p-P62 (S349) and P62 than uninfected cells. These changes were reversed with FGFR4 siRNA knockdown. E) representative images of immunohistochemistry staining of FGFR4 and NRF2 in serial tissue sections from coded human gastric tissues with normal histology (NG), high grade dysplasia (HGD) and cancer. Original magnification 10× and 40X are shown on the left side of the panel). A progressive increase in FGFR4 and NRF2 was observed along different histological pathologies (HGD and cancer) as compared to NG. F-G) The graph bars summarize the immunohistochemical staining index scores according to the number of cases in percentage for each histological stage on the gastric tissue microarrays. We used Cochran-Mantel-Haenszel Statistical analysis of disease to analyze IHC scores across histological stages, FGFR4 ($X^2 = 41.28$, Df = 2, $P < 0.0001$) and NRF2 ($X^2 = 12.3$, Df = 2, $P < 0.01$). H) Spearman's Correlation analysis shows a positive correlation between FGFR4 and NRF2 index scores in gastric cancer tissues.

demonstrated significant overexpression of FGFR4, NRF2 and P62 with progression across histological stages [FGFR4 ($X^2 = 41.28$, Df = 2, $P < 0.0001$, Fig. 8F), NRF2 ($X^2 = 12.30$, Df = 2, $P < 0.001$, Fig. 8G), and P62 ($X^2 = 57.17$, Df = 2, $P < 0.0001$) (Supplemental Fig. 10B). Moreover, using Spearman's Correlation analysis, a significant correlation was present between FGFR4 and NRF2 in the gastric cancer group (Fig. 8H, $R^2 = 0.24$ and $P < 0.0001$). Also, we found a significant correlation between FGFR4 and P62 (Supplemental Fig. 10C, $R^2 = 0.16$ and $P < 0.01$) and between NRF2 and P62 (Supplemental Fig. 10D, $R^2 = 0.12$ and $P < 0.01$). in the TMA samples of gastric cancer group. A cartoon summarizing the findings is illustrated in Fig. 9.

4. Discussion

Gastric cancer is mediated by complex cellular and molecular changes that are mediated by several endogenous and environmental factors that induce oxidative stress [34,35]. *H. pylori* infection, a leading risk factor for gastric carcinogenesis, generates high levels of ROS and oxidative stress [36]. Under homeostatic conditions, cells develop adaptive protective antioxidant mechanisms to maintain oxidative stress below lethal levels. On the other hand, moderate levels of ROS and oxidative stress tend to promote cell survival and neoplastic growth [37,38].

FGFR4 is overexpressed in several cancer types, including gastric cancer [15,39]. A recent study has shown that FGFR4 is the most significantly overexpressed FGFR family member in gastric cancer [15]. Our findings demonstrate a functional mechanistic link between *H. pylori* infection, FGFR4 expression, and NRF2 protein level and activity.

H. pylori infection induces high levels of ROS and oxidative stress in gastric carcinogenesis [36]. Sustained and uncontrolled high ROS levels are known to be lethal not only to gastric mucosa cells but also to *H. pylori* bacteria [40]. Our analysis of gastric cancer databases showed an association between FGFR4 and oxidative stress molecular signature. We have previously shown an increase in FGF ligand and FGFR4 activation in response to *H. pylori* [15]. Therefore, we investigated if FGFR4 plays a role in controlling the toxic high levels of ROS and oxidative stress. Our results demonstrate an antioxidant role of FGFR4 where its expression reduced the levels of reactive oxygen species in response to *H. pylori* infection. In fact. the knockdown of FGFR4 led to a decrease in NRF2, impairing one of the major cellular antioxidant mechanisms. We observed accumulation and increase of *H. pylori-induced* ROS levels with an increase in DNA damage in absence of FGFR4. Therefore, the induction of FGFR4 in response to *H. pylori* induces not only the oncogenic functions [17–19], but also cellular protective mechanisms to control ROS levels, contributing to the persistence of infection and cell survival.

NRF2, known as the master antioxidant transcription factor, plays an essential role in cellular homeostasis. NRF2 functions as a double sword where it can be anti-tumorigenic in normal cells or pro-tumorigenic in neoplastic cells, depending on the stimulus and cell context [41,42]. We detected a significant association between FGFR4 levels and the molecular signature of NRF2 in gastric cancer tissue samples and in response to *H. pylori* infection in *in vitro* models and mouse models. We also detected high levels of FGFR4 and NRF2 in the TFF1 KO mouse

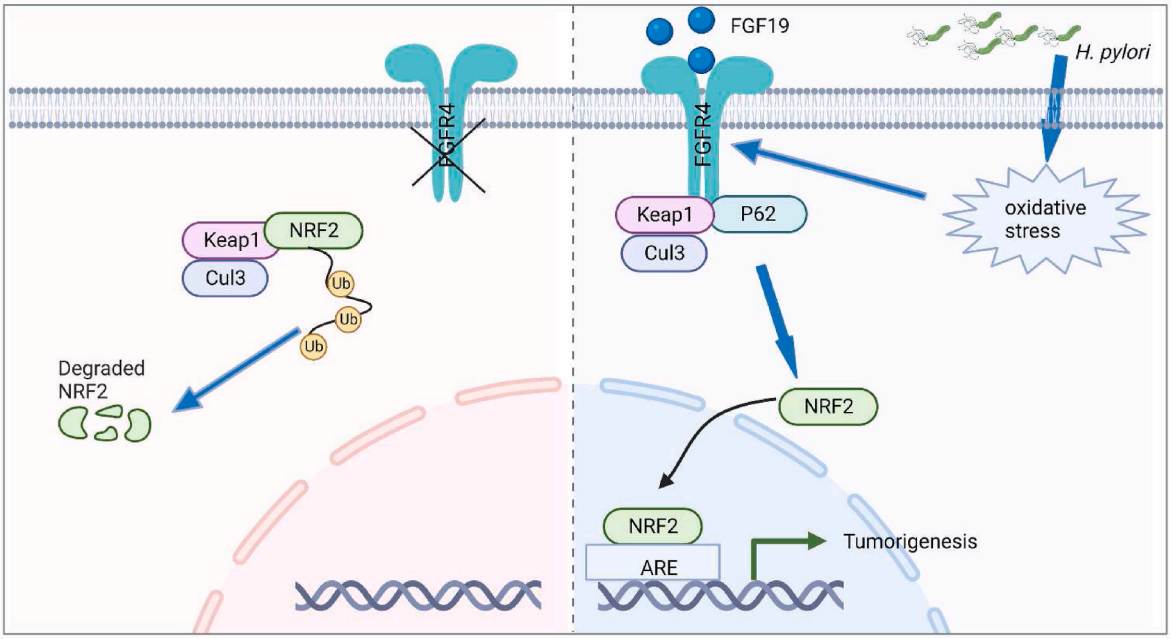

Fig. 9. A schematic diagram illustrating the role of FGFR4 in activating and stabilizing NRF2. Exposure of cells to *H. pylori* infection induces oxidative stress and FGFR4 expression. FGFR4 binds to P62. The FGFR4-P62 complex binds to KEAP1 in NRF2 degradation complex, competing with binding of KEAP1 top NRF2. NRF2 escapes degradation, accumulates, and translocates to the nucleus to induce transcription of antioxidant response genes.

model of chronic inflammation and gastric tumorigenesis, similar to human [20,27]. Indeed, we showed that activation of FGFR4-NRF2 axis is a plausible antioxidant system that counteracts the accumulation of ROS to maintain cellular homeostasis.

The *in vitro* and *in vivo* results suggested an important role for FGFR4 in promoting NRF2 accumulation and activity in response to infection. P62 is known to compete with NRF2 binding on KEAP1. This step allows NRF2 to escape KEAP1-dependent ubiquitination and proteasomal degradation via KEAP1-Cul3 complex with subsequent accumulation, nuclear translocation, and transcription activation [9,36,43]. In this study, we showed the regulation of NRF2 by FGFR4 via a P62-dependent mechanism where FGFR4 forms a complex with KEAP1 and P62, in response to *H. pylori* infection. We also found that FGFR4 induced an increase in P62 which interfered with the canonical mechanisms for regulation of NRF2 via KEAP1-dependent mechanisms. The increase in phospho-P62 was consistent with the increase in the total levels, suggesting that the increase in P62 was the primary event triggered by FGFR4, whereas its phosphorylation was likely mediated by the other cellular mechanisms. In this regards, P62 is known to undergo phosphorylation by mTOR or AKT; two kinases commonly activated in gastric cancer [44].

We confirmed the role of FGFR4 in regulating NRF2 where FGFR4 knockdown or pharmacologic inhibition (H3B-6527) reversed the NRF2 activity in both *in vitro* and *in vivo* system models. As expected, this was associated with an increase in ROS and cell death. Although we did not investigate the therapeutic impact of FGFR4 inhibitors in this study, gastric cancer patients with high levels of FGFR4 or NRF2 are known to be resistant to chemotherapeutics [45–47]. FGFR4 high levels are also associated with poor clinical outcomes in gastric cancer [15,48]. In this context, our findings illustrate a previously unknown potentially druggable link between infection, FGFR4 and NRF2 levels that can explain inherent chemotherapeutic resistance in gastric cancer.

5. Conclusion

High levels of FGFR4 and NRF2 are associated with poor clinical outcomes in gastric cancer. Induction of FGFR4 in response to *H. pylori* infection mediates activation of the NRF2 antioxidant response to protect against the accumulation of infection-induced high levels of ROS. Accumulation and activation of NRF2 is mediated by an interaction between FGFR4 and P62 that competes with NRF2 binding to KEAP1, allowing NRF2 to escape degradation. The FGFR4-NRF2 axis is a potential druggable vulnerability that can be targeted with FGFR4 inhibitors, calling for additional studies to validate this therapeutic concept.

Ethics approval and consent to participate

All samples were de-identified and considered non-human subjects research in accordance with NIH and institutional guidelines.

Consent for publication

Not applicable.

Availability of data and materials

All data generated or analyzed during this study are included in this published article and its supplementary information files.

Funding

This study was partially supported by grants awarded to WER from the U.S. Department of Veterans Affairs (1IK6BX003787 and I01BX001179) and the U.S. National Cancer Institute (NCI) (R01CA24994 and R01CA266528). The use of flow cytometry (SCR_022501), cancer modeling (SCR_022891), and bioinformatics (SCR_022890) shared resources was supported by the NCI-funded Sylvester Comprehensive Cancer Center (P30CA240139). This work's content is solely the responsibility of the authors. It does not necessarily represent the official views of the Department of Veterans Affairs, National Institutes of Health, or the University of Miami.

Authors' contributions

Conceptualization: WER and MS conceived and supervised the project. MS and XZ performed key experiments and drafted the manuscript. OE-G provided support for cell culture and RNA purifications. ZC and HL provided support and troubleshooting of experiments and molecular techniques. SM and MG assisted with tissue culture. NB an SZ assisted in *H. pylori* culture, and luciferase assay. LC and XSC assisted with statistical and bioinformatics analysis. OGM evaluated the mouse and human tissue histology. DP provided support with immunohistochemistry analysis. ZX assisted in the drafting of the manuscript. All authors read and approved the final manuscript.

Declaration of competing interest

The authors declare that they have no competing interests.

Acknowledgements

We thank Dr. Richard M. Peek (Vanderbilt University Medical Center) for providing the *H. pylo*ri strains used in this study.

Abbreviation

FGFR4	Fibroblast growth factor receptor-4
ROS	Reactive oxygen species
NRF2	Nuclear factor-erythroid 2-related factor
H. pylori	*Helicobacter pylori*
FGF19	Fibroblast growth factor 19
HO1	Heme oxygenase 1
KEAP1	Kelch-like ECH-associated protein 1
TFF1	Trefoil Factor 1

Appendix A. Supplementary data

Supplementary data to this article can be found online at https://doi.org/10.1016/j.redox.2023.102998.

References

[1] R.L. Siegel, K.D. Miller, H.E. Fuchs, A. Jemal, Cancer statistics, 2022, Ca - Cancer J. Clin. 72 (1) (2022) 7–33.
[2] H. Sung, J. Ferlay, R.L. Siegel, M. Laversanne, I. Soerjomataram, A. Jemal, et al., Global cancer statistics 2020: GLOBOCAN estimates of incidence and mortality worldwide for 36 cancers in 185 countries, Ca - Cancer J. Clin. 71 (3) (2021) 209–249.
[3] T. Ugai, N. Sasamoto, H.Y. Lee, M. Ando, M. Song, R.M. Tamimi, et al., Is early-onset cancer an emerging global epidemic? Current evidence and future implications, Nat. Rev. Clin. Oncol. 19 (10) (2022) 656–673.
[4] F.I. Bussiere, V. Michel, J. Fernandes, L. Costa, V. Camilo, G. Nigro, et al., DNA hypermethylation downregulates telomerase reverse transcriptase (TERT) during H. Pylori-induced chronic inflammation, JAMA Oncol. 2019 (2019), 5415761.
[5] O. Handa, Y. Naito, T. Yoshikawa, Helicobacter pylori: a ROS-inducing bacterial species in the stomach, Inflamm. Res. 59 (12) (2010) 997–1003.
[6] U. Jain, K. Saxena, N. Chauhan, Helicobacter pylori induced reactive oxygen Species: a new and developing platform for detection, Helicobacter 26 (3) (2021), e12796.
[7] Y. Teng, H. Zhao, L. Gao, W. Zhang, A.Y. Shull, C. Shay, FGF19 protects hepatocellular carcinoma cells against endoplasmic reticulum stress via activation of FGFR4-GSK3beta-Nrf2 signaling, Cancer Res. 77 (22) (2017) 6215–6225.
[8] K. Itoh, N. Wakabayashi, Y. Katoh, T. Ishii, K. Igarashi, J.D. Engel, et al., Keap1 represses nuclear activation of antioxidant responsive elements by Nrf2 through binding to the amino-terminal Neh2 domain, Genes Dev. 13 (1) (1999) 76–86.

[9] I. Ganan-Gomez, Y. Wei, H. Yang, M.C. Boyano-Adanez, G. Garcia-Manero, Oncogenic functions of the transcription factor Nrf2, Free Radic. Biol. Med. 65 (2013) 750–764.
[10] M. Katoh, Fibroblast growth factor receptors as treatment targets in clinical oncology, Nat. Rev. Clin. Oncol. 16 (2) (2019) 105–122.
[11] S. Thomson, F. Petti, I. Sujka-Kwok, D. Epstein, J.D. Haley, Kinase switching in mesenchymal-like non-small cell lung cancer lines contributes to EGFR inhibitor resistance through pathway redundancy, Clin. Exp. Metastasis 25 (8) (2008) 843–854.
[12] N. Turner, R. Grose, Fibroblast growth factor signalling: from development to cancer, Nat. Rev. Cancer 10 (2) (2010) 116–129.
[13] M. Korc, R.E. Friesel, The role of fibroblast growth factors in tumor growth, Curr. Cancer Drug Targets 9 (5) (2009) 639–651.
[14] Y. Liu, M. Cao, Y. Cai, X. Li, C. Zhao, R. Cui, Dissecting the role of the FGF19-FGFR4 signaling pathway in cancer development and progression, Front. Cell Dev. Biol. 8 (2020) 95.
[15] X. Zhang, M. Soutto, Z. Chen, N. Bhat, S. Zhu, M.F. Eissmann, et al., Induction of fibroblast growth factor receptor 4 by Helicobacter pylori via signal transducer and activator of transcription 3 with a feedforward activation loop involving SRC signaling in gastric cancer, Gastroenterology 163 (3) (2022) 620–636 e9.
[16] I. Uriarte, M.U. Latasa, S. Carotti, M.G. Fernandez-Barrena, O. Garcia-Irigoyen, M. Elizalde, et al., Ileal FGF15 contributes to fibrosis-associated hepatocellular carcinoma development, Int. J. Cancer 136 (10) (2015) 2469–2475.
[17] X. Yu, N. Yan, Z. Li, Y. Hua, W. Chen, FGF19 sustains the high proliferative ability of keratinocytes in psoriasis through the regulation of Wnt/GSK-3beta/beta-catenin signalling via FGFR4, Clin. Exp. Pharmacol. Physiol. 46 (8) (2019) 761–769.
[18] L. Lang, Y. Teng, Fibroblast growth factor receptor 4 targeting in cancer: new insights into mechanisms and therapeutic strategies, Cells 8 (1) (2019).
[19] A. Raja, I. Park, F. Haq, S.M. Ahn, FGF19-FGFR4 signaling in hepatocellular carcinoma, Cells 8 (6) (2019).
[20] M. Soutto, A. Belkhiri, M.B. Piazuelo, B.G. Schneider, D. Peng, A. Jiang, et al., Loss of TFF1 is associated with activation of NF-kappaB-mediated inflammation and gastric neoplasia in mice and humans, J. Clin. Invest. 121 (5) (2011) 1753–1767.
[21] O. Lefebvre, M.P. Chenard, R. Masson, J. Linares, A. Dierich, M. LeMeur, et al., Gastric mucosa abnormalities and tumorigenesis in mice lacking the pS2 trefoil protein, Science 274 (5285) (1996) 259–262.
[22] T.A. Nagy, M.R. Frey, F. Yan, D.A. Israel, D.B. Polk, R.M. Peek Jr., Helicobacter pylori regulates cellular migration and apoptosis by activation of phosphatidylinositol 3-kinase signaling, J. Infect. Dis. 199 (5) (2009) 641–651.
[23] R.M. Barrozo, C.L. Cooke, L.M. Hansen, A.M. Lam, J.A. Gaddy, E.M. Johnson, et al., Functional plasticity in the type IV secretion system of Helicobacter pylori, PLoS Pathog. 9 (2) (2013), e1003189.
[24] W. El-Rifai, C.A. Moskaluk, M.K. Abdrabbo, J. Harper, C. Yoshida, G.J. Riggins, et al., Gastric cancers overexpress S100A calcium-binding proteins, Cancer Res. 62 (23) (2002) 6823–6826.
[25] A. Bartha, B. Gyorffy, TNMplot.com: a web tool for the comparison of gene expression in normal, tumor and metastatic tissues, Int. J. Mol. Sci. 22 (5) (2021).
[26] S. Chaithongyot, M. Naumann, Helicobacter pylori-induced reactive oxygen species direct turnover of CSN-associated STAMBPL1 and augment apoptotic cell death, Cell. Mol. Life Sci. 79 (2) (2022) 86.
[27] M. Soutto, Z. Chen, A.A. Bhat, L. Wang, S. Zhu, A. Gomaa, et al., Activation of STAT3 signaling is mediated by TFF1 silencing in gastric neoplasia, Nat. Commun. 10 (1) (2019) 3039.
[28] J.J. Joshi, H. Coffey, E. Corcoran, J. Tsai, C.L. Huang, K. Ichikawa, et al., H3B-6527 is a potent and selective inhibitor of FGFR4 in FGF19-driven hepatocellular carcinoma, Cancer Res. 77 (24) (2017) 6999–7013.
[29] R. Roskoski Jr., The role of fibroblast growth factor receptor (FGFR) protein-tyrosine kinase inhibitors in the treatment of cancers including those of the urinary bladder, Pharmacol. Res. 151 (2020), 104567.
[30] S. Wu, H. Lu, Y. Bai, Nrf2 in cancers: a double-edged sword, Cancer Med. 8 (5) (2019) 2252–2267.
[31] S. Menegon, A. Columbano, S. Giordano, The dual roles of NRF2 in cancer, Trends Mol. Med. 22 (7) (2016) 578–593.
[32] K. Taguchi, M. Yamamoto, The KEAP1-NRF2 system in cancer, Front. Oncol. 7 (2017) 85.
[33] T.F. Tsai, P.C. Chen, Y.C. Lin, K.Y. Chou, H.E. Chen, C.Y. Ho, et al., Miconazole contributes to NRF2 activation by noncanonical P62-KEAP1 pathway in bladder cancer cells, Drug Des. Dev. Ther. 14 (2020) 1209–1218.
[34] F. Avila, C. Theoduloz, C. Lopez-Alarcon, E. Dorta, G. Schmeda-Hirschmann, Cytoprotective mechanisms mediated by polyphenols from Chilean native berries against free radical-induced damage on AGS cells, Oxid. Med. Cell. Longev. 2017 (2017), 9808520.
[35] J. Kanner, J. Selhub, A. Shpaizer, B. Rabkin, I. Shacham, O. Tirosh, Redox homeostasis in stomach medium by foods: the Postprandial Oxidative Stress Index (POSI) for balancing nutrition and human health, Redox Biol. 12 (2017) 929–936.
[36] L.D. Butcher, G. den Hartog, P.B. Ernst, S.E. Crowe, Oxidative stress resulting from Helicobacter pylori infection contributes to gastric carcinogenesis, Cell Mol. Gastroenterol. Hepatol. 3 (3) (2017) 316–322.
[37] J.D. Hayes, A.T. Dinkova-Kostova, K.D. Tew, Oxidative stress in cancer, Cancer Cell 38 (2) (2020) 167–197.
[38] S.K. Chiang, S.E. Chen, L.C. Chang, The role of HO-1 and its crosstalk with oxidative stress in cancer cell survival, Cells 10 (9) (2021).
[39] H. Xie, D.M. Alem Glison, R.D. Kim, FGFR4 inhibitors for the treatment of hepatocellular carcinoma: a synopsis of therapeutic potential, Expet Opin. Invest. Drugs 31 (4) (2022) 393–400.
[40] J.D. Lambeth, NOX enzymes and the biology of reactive oxygen, Nat. Rev. Immunol. 4 (3) (2004) 181–189.
[41] D. Peng, A. Zaika, J. Que, W. El-Rifai, The antioxidant response in Barrett's tumorigenesis: a double-edged sword, Redox Biol. 41 (2021), 101894.
[42] E. Panieri, A. Buha, P. Telkoparan-Akillilar, D. Cevik, D. Kouretas, A. Veskoukis, et al., Potential applications of NRF2 modulators in cancer therapy, Antioxidants 9 (3) (2020).
[43] D. Yasuda, T. Ohe, K. Takahashi, R. Imamura, H. Kojima, T. Okabe, et al., Inhibitors of the protein-protein interaction between phosphorylated p62 and Keap1 attenuate chemoresistance in a human hepatocellular carcinoma cell line, Free Radic. Res. 54 (11–12) (2020) 859–871.
[44] P. Sanchez-Martin, T. Saito, M. Komatsu, p62/SQSTM1: 'Jack of all trades' in health and cancer, FEBS J. 286 (1) (2019) 8–23.
[45] J. Bao, J. Li, D. Li, Z. Li, Correlation between expression of NF-E2-related factor 2 and progression of gastric cancer, Int. J. Clin. Exp. Med. 8 (8) (2015) 13235–13242.
[46] T. Farkhondeh, A.M. Pourbagher-Shahri, M. Azimi-Nezhad, F. Forouzanfar, A. Brockmueller, M. Ashrafizadeh, et al., Roles of Nrf2 in gastric cancer: targeting for therapeutic strategies, Molecules 26 (11) (2021).
[47] H. Chen, D.P. Shen, Z.Z. Zhang, J.H. Liu, Y.Y. Shen, X.Z. Ni, Fibroblast growth factor receptor 4 protein expression and clinicopathological features in gastric cancer, World J. Gastroenterol. 21 (6) (2015) 1838–1844.
[48] Y.W. Ye, X. Zhang, Y. Zhou, J. Wu, C. Zhao, L. Yuan, et al., The correlations between the expression of FGFR4 protein and clinicopathological parameters as well as prognosis of gastric cancer patients, J. Surg. Oncol. 106 (7) (2012) 872–879.
[49] Y. Mitsuishi, K. Taguchi, Y. Kawatani, T. Shibata, T. Nukiwa, H. Aburatani, et al., Nrf2 redirects glucose and glutamine into anabolic pathways in metabolic reprogramming, Cancer Cell 22 (1) (2012) 66–79.